

High-spin and low-spin f - d transitions of Tb^{3+} in elpasolite hosts

Lixin Ning,¹ Chris S. K. Mak,² and Peter A. Tanner²¹*Electronics Design Division, Department of Information Technology and Media, Mid-Sweden University, SE-851 70 Sundsvall, Sweden*²*Department of Biology and Chemistry, City University of Hong Kong, Tat Chee Avenue, Kowloon, Hong Kong S.A.R., People's Republic of China*

(Received 23 May 2005; published 19 August 2005)

The electronic absorption spectra of $Cs_2NaTbCl_6$ and $Cs_2NaYCl_6:Tb^{3+}$ have been recorded between 34 000–43 000 cm^{-1} at temperatures down to 10 K. Well-resolved spin-forbidden and spin-allowed transitions are observed, comprising three and one electronic transitions, respectively, between the crystal field levels of $4f^8$ and $4f^7d$ (t_{2g}) states. For transitions from the electronic ground state, symmetry selection rules restrict the upper crystal field levels to be Γ_{4u} (T_{1u}) symmetry. Three vibrational progression modes appear in the electronic transitions and these are assigned to breathing modes with the first, second, and third nearest neighbors of Tb^{3+} . The experimental results are rationalized both from the use of a simple model and from the extended f -shell programs of Reid. The excitation process $4f^8 \rightarrow 4f^75d$ (t_{2g}) involves a small (5.5 pm) bond length change which is considered to be a contraction rather than an expansion.

DOI: 10.1103/PhysRevB.72.085127

PACS number(s): 71.70.Ch, 33.20.Lg, 33.70.-w

I. INTRODUCTION

Recently, van Pieterse *et al.* have studied the VUV emission and excitation spectra of different lanthanide ions (Ln^{3+}) doped into the $LiYF_4$, CaF_2 , and YPO_4 crystals, using synchrotron radiation as the excitation source.¹⁻⁴ It was found that the electric dipole strength for the f - d transition decreases across the lanthanide series and that for the later $4f^N$ ($N > 7$) members that the splitting between the high- and low-spin fd states decreases across the series. However, most of the spectra comprised broad features (as is the case for other systems, e.g., Ref. 5), and in particular the $CaF_2:Ln^{3+}, Na^+$ spectra showed the presence of several sites. Furthermore, one problem inherent in excitation spectra is the possibility that bands are not due to the bulk material, but arise from energy transfer from other species. Electronic absorption spectra do not exhibit such features. Earlier studies of the low-spin and high-spin $4f^8 \rightarrow 4f^75d^1$ absorption spectra of Tb^{3+} have been made for $YPO_4:Tb^{3+}$,⁶ $TbCl_6^{3-}$ in mixed succinonitrile-ethanonitrile solution,⁷ Tb^{3+} in dilute $HClO_4$ solution,⁸ and in other studies summarized by Shi and Zhang.⁹

Most of the systems previously chosen for investigation of f - d transitions have lanthanide ions at sites of low symmetry so that electronic energy levels are nondegenerate in the case of f^N (N even). Furthermore, the molecular point group selection rules may permit transitions between all f and d states to be potentially active, thus leading to spectral consequences of band congestion and broadening. This is not the case for Ln^{3+} situated in $Fm\bar{3}m$ elpasolite host lattices, where the site symmetry is octahedral O_h . For f^N (N even), the electronic degeneracy can be up to threefold, and the point group selection rule for an electric dipole transition between initial (i) and final (f) states:

$$\Gamma(i) \times \Gamma(f) \text{ contains } \Gamma(D^{(1)}), \quad (1)$$

where $D^{(1)}$ is the electric dipole moment operator, excludes many transitions. Thus, compared with the low symmetry

systems, not only are the numbers of energy levels reduced but also the numbers of allowed f - d electronic transitions are smaller. It is therefore anticipated that simpler, more clearly resolved spectra would ensue.

Thus, well-resolved f - d electronic absorption transitions have recently been reported for the lanthanide ions Ce^{3+} and Pr^{3+} doped into the hexachloroelpasolite Cs_2NaYCl_6 lattice.¹⁰ This has enabled conclusions to be deduced concerning the symmetry representations of the crystal field levels involved in the f - d transitions. Furthermore, analyses and interpretations of the associated vibronic structure have also been possible.

It is the object of this paper to investigate the f - d spectra of Tb^{3+} in this cubic lattice. The f - f one-^{11,12} and two-photon¹³ spectra of Tb^{3+} have been extensively investigated in $Cs_2NaTbCl_6$, also in the context of energy transfer to Eu^{3+} .¹⁴⁻¹⁶ Although *neat* $Cs_2NaTbCl_6$ undergoes a phase transition from the cubic $Fm\bar{3}m$ structure below 20 K, the diluted $Cs_2NaYCl_6:Tb^{3+}$ systems retain cubic symmetry at 10 K.

II. EXPERIMENTAL

Polycrystalline samples of $Cs_2NaTbCl_6$ and $Cs_2NaY_{1-x}Tb_xCl_6$ ($x=0.01, 0.0001$) were prepared according to Morss method *E* (Ref. 17) by dissolving Tb_4O_7 (99.9%; Strem) and Y_2O_3 (99.999%; Strem) in hot concentrated hydrochloric acid. Then $CsCl$ (99.999%) and $NaCl$ (99.999%) were added and the clear solution was evaporated to dryness. The powder was transferred to a preheated, clean quartz tube, and heated under vacuum inside a tube furnace at 723 K for two days and then sealed off as an ampoule. The ampoule was lowered through the Bridgman furnace at 1123 K at a rate 1.2 cm/h. The tube was opened after it had completely passed through the furnace. The crystal was cut and polished for spectroscopic measurements.

Ultraviolet spectra were recorded in the single beam mode using a D_2 or Xe lamp as the external light source, with

TABLE I. Vibrational data for $\text{Cs}_2\text{NaTbCl}_6$. irrep.: irreducible representation; str.: stretch; sym.: symmetric; ant.: antisymmetric; trans.: translatory.

Unit cell group mode (Ref. 18) and O_h point group irrep.	Moiety mode and O_h point group irrep.	20 K Raman spectrum	10 K f - f vibronic spectra
S_1 Tb—Cl sym. str.	ν_1 (α_{1g})	290	
S_2 Tb—Cl str.	ν_2 (ϵ_g)	232	
S_3 rotatory lattice (τ_{1g})			
S_4 Cl—Tb—Cl bend	ν_5 (τ_{2g})	122	
S_5 Cs transl. (τ_{2g})		44	
S_6 Tb—Cl ant. str.	ν_3 (τ_{1u})		244, 259, 285
S_7 Cl—Tb—Cl bend	ν_4 (τ_{1u})		103, 116, 129
S_8 Na—Cl str. (τ_{1u})			182
S_9 Cs transl. (τ_{1u})			55
S_{10} Cl—Tb—Cl bend	ν_6 (τ_{2u})		72, 81

resolution 2–4 cm^{-1} by an Acton 0.5 m monochromator, having an 1800 grooves/mm grating blazed at 250 nm, and a back-illuminated SpectruMM CCD detector. Calibrations were made to vacuum wave numbers by a low-pressure mercury lamp. All the spectra were recorded between 300–10 K with the polished polycrystalline sample housed in an Oxford Instruments closed cycle cryostat, with base temperature 10 K.

III. RESULTS AND DISCUSSION

The electronic ground state of the $4f^8$ configuration of Tb^{3+} in octahedral symmetry is ${}^7F_6\Gamma_1$. The normal vibrations of the $\text{Cs}_2\text{NaTbCl}_6$ crystal are described in the notation of Lentz,^{10,18} with the relationship to the TbCl_6^{3-} moiety mode vibrations being given in Table I. Vibrational assignments are included from the low temperature Raman and f^8 - f^8 vibronic spectra. The energies of the stretching vibrations are somewhat higher in the $\text{Cs}_2\text{NaYCl}_6$ lattice than in $\text{Cs}_2\text{NaTbCl}_6$, with ν_1 , for example, being near 300 cm^{-1} .

When one electron is promoted to the lowest d -electron level, the excited configuration is $4f^75d^1$ and the $4f$ orbital becomes half filled. This configuration stabilizes the lowest $5d$ state and makes it low lying, which is similar to the case of Ce^{3+} ($4f^1 \rightarrow 4f^05d^1$). Two sets of absorption bands are observed in neat $\text{Cs}_2\text{NaTbCl}_6$ at around 35 000 cm^{-1} and 42 000 cm^{-1} , and they are assigned as spin-forbidden (7F_6 - 9D) and spin-allowed (7F_6 - 7D) $4f \rightarrow 5d$ transitions, respectively, with Hund's rule placing the former at lower energy. It is interesting that the crystal field levels of the outer d electron are inverted in octahedral symmetry in comparison with $\text{CaF}_2:\text{Tb}^{3+}$ and $\text{LiYF}_4:\text{Tb}^{3+}$, so that for the core-outer electron representation $4f^{N-1}5d$, the (8S) ${}^2t_{2g}$ states lie below (8S) 2e_g . By contrast to forbidden f - f electronic transitions, f - d transitions are orbitally allowed to first order. However, since the ground state $4f^8$ crystal field level of Tb^{3+} is Γ_{1g} , from Eq. (1) only the ${}^7F_6\Gamma_{1g} \rightarrow \Gamma_{4u}$ ($4f^{N-1}5d$) transitions are allowed in O_h symmetry. Figure 1 shows the survey 10 K absorption spectrum of TbCl_6^{3-} between 34 000 and 45 000 cm^{-1} . The molar extinction coefficients (in

$\text{mol}^{-1} \text{l cm}^{-1}$) of the two groups of bands have been measured in mixed ethanonitrile-succinonitrile solution⁷ as 28 (9D , high spin) and 1500 (7D , low spin) showing the importance of the $\Delta S=0$ selection rule for an electric dipole transition.

A. Spin-forbidden $4f^8 \rightarrow 4f^75d^1$ transition

The 9D state comprises the following crystal field levels (all u): $2\Gamma_1 + 2\Gamma_2 + 4\Gamma_3 + 5\Gamma_4 + 6\Gamma_5$, but this includes not only the coupling of the core ${}^8S_{7/2}$ with the $5d^1$ ${}^2t_{2g}$ state, but also with the 2e_g state. The states arising from the coupling with the ${}^2t_{2g}$ state exclusively are shown in Fig. 2(a).

Figure 3 shows the 10 K absorption spectra of (a) $\text{Cs}_2\text{NaYCl}_6:\text{Tb}^{3+}$ (1 mol %) and (b) $\text{Cs}_2\text{NaTbCl}_6$. The lowest energy zero phonon line (ZPL) is labeled I in Fig. 3(a) and is located at 34 332 cm^{-1} . It is assigned to the transition from the ${}^7F_6\Gamma_{1g}$ ($4f^8$) ground state to the first Γ_{4u} level of 9D ($4f^75d^1$). Progressions in three vibrational modes are observed based upon this electronic origin. The vibrational intervals of 297 ± 2 , 170 ± 2 , and 46 cm^{-1} are associated with breathing modes of Tb^{3+} with the first, second, and third nearest neighbors.¹⁰ Two higher-energy transitions II, III are

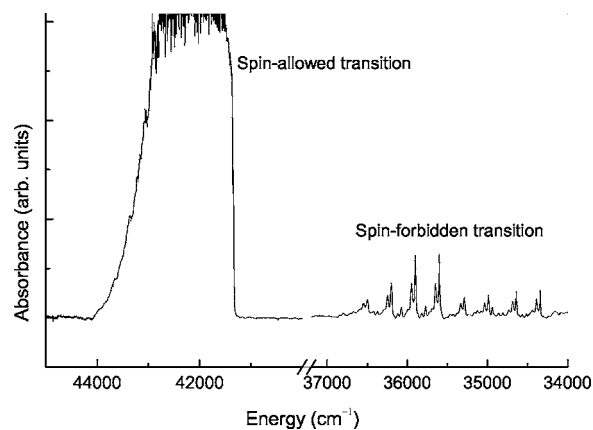


FIG. 1. 10 K survey absorption spectrum of $\text{Cs}_2\text{NaY}_{0.99}\text{Tb}_{0.01}\text{Cl}_6$.

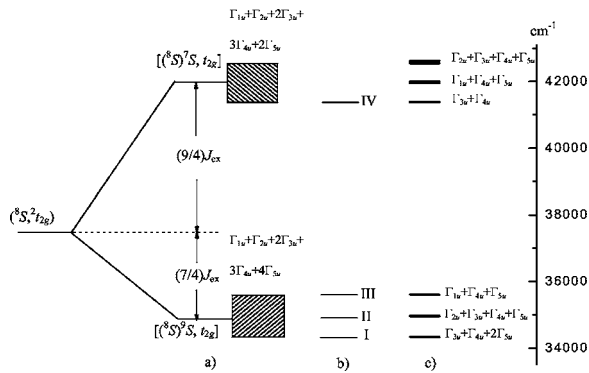


FIG. 2. Schematic diagram of the energy levels of $4f^7 5d$. (a) shows the energy levels from a simple model analysis. Only the levels arising from the coupling of the $4f^7$ core state 8S with the $5d^1 2t_{2g}$ state are included. (b) gives the energies positions for the four observed Γ_{4u} levels (I–IV). (c) shows the energy levels from calculations in the spectral range of 34 000–43 000 cm^{-1} . The irreducible representations of the levels are also included for comparison with those from simple model analysis and experiment.

also clearly located (Fig. 3) with the Γ_{4u} electronic origins located at 34 982 and 35 590 cm^{-1} . The energy difference between I and III is 1258 cm^{-1} .

There are additional weak bands at $38 \pm 4 \text{ cm}^{-1}$ to low energy of the $\Gamma_{1g} \rightarrow \Gamma_{4u}$ electronic origins, for which the relative intensity increases with temperature, and these are assigned to hot transitions from ${}^7F_6 \Gamma_{4g}$ ($4f^8$) state,^{13,16} as well as to the 46 cm^{-1} vibrational hot bands. Additional bands are expected to be observed for transitions from the Γ_{4g} level to excited Γ_{5u} and Γ_{3u} levels, but these transitions are not observed because either they are too weak or they are masked by the structure of the $\Gamma_{1g} \rightarrow \Gamma_{4u}$ transitions. The subsequent calculations (Sec. IV) confirm both of these presumptions.

The 10 K absorption spectrum of *neat* $\text{Cs}_2\text{NaTbCl}_6$, as shown in Fig. 3(b), exhibits total absorption for the middle part. The weak, highest-energy vibrational progressions are more clearly observed than in Fig. 3(a) and have the progression interval of 298 cm^{-1} . The lowest energy ${}^7F_6 \Gamma_{1g} \rightarrow \Gamma_{4u}(4f^7 5d^1)$ origin is at 34 364 cm^{-1} , and the weaker feature to low energy is assigned to a hot band as above. It is interesting that this low spin group of bands overlaps $4f^8$ - $4f^8$ transitions, as determined from two-photon spectra.¹³ In fact, the ${}^7F_6 \rightarrow {}^5H_4$ group of bands is coincident with the onset of the $4f^8 \rightarrow 4f^7 5d^1$ group, but is expected to be much weaker in intensity. Thus the strict $g \rightarrow g$ selection rule does not lead to the participation of $4f^7 5d^1$ levels in the two-photon f - f spectra, whereas the nonradiative relaxation from $4f^7 5d^1$ to $4f^8$ levels leads to the absence of emission from $4f^7 5d^1$.

B. Spin-allowed $4f^8 \rightarrow 4f^7 5d^1$ transition

The crystal field states derived from 7D by coupling the core 8S with $5d^1 2t_{2g}$ are shown in Fig. 2(a). The first ZPL of the spin-allowed f - d transition is at about 7050 cm^{-1} higher energy than that of the spin-forbidden transition, which compares with the low-spin and high-spin splittings (in cm^{-1}) of

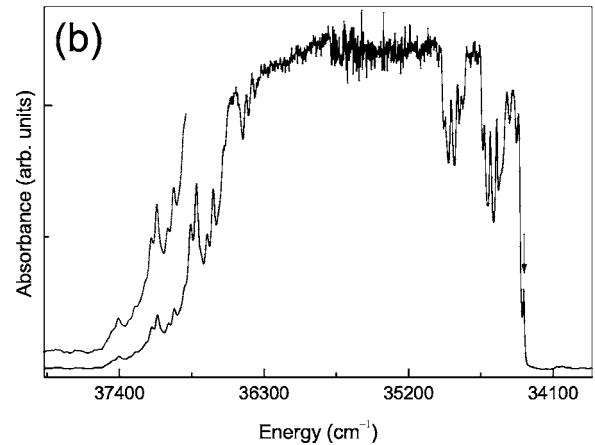
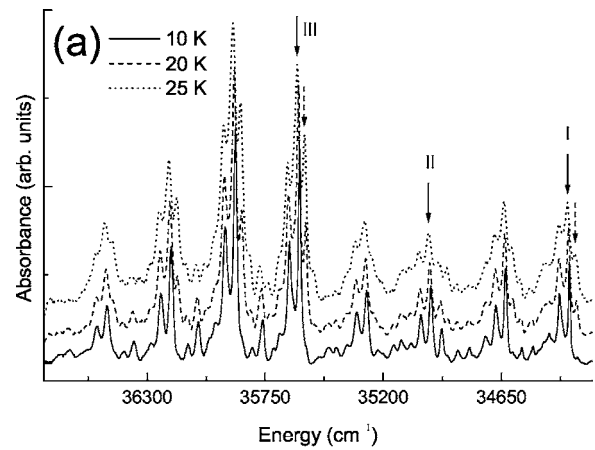


FIG. 3. Absorption spectra of spin-forbidden transitions in (a) $\text{Cs}_2\text{NaYCl}_6:\text{Tb}^{3+}$ (1 mol %) at different temperatures and (b) $\text{Cs}_2\text{NaTbCl}_6$ at 10 K. The electronic origins in (a) are marked with arrows.

7995, 7920, 7370 reported for Tb^{3+} in the hosts LiYF_4 , CaF_2 , and YPO_4 , respectively,¹⁰ and an average value for 19 compounds of 6300 ± 900 .⁹ The 10 K absorption spectra of $\text{Cs}_2\text{NaYCl}_6:\text{Tb}^{3+}$ (0.01 mol %) and $\text{Cs}_2\text{NaTbCl}_6$ are shown in Figs. 4(a) and 4(b), respectively. Figure 4(a) also shows the ${}^7F_6 \Gamma_{1g} \rightarrow {}^7D \Gamma_{4u}$ transition at different temperatures. The origin located at 41 380 cm^{-1} in the 10 K spectrum is assigned as the lowest energy $\Gamma_{1g} \rightarrow \Gamma_{4u}$ origin for the spin allowed $4f^8 \rightarrow 4f^7 5d^1$ transitions. Well-defined vibration progressions based upon this origin are clearly observed, with energies 47, 171, and 298 cm^{-1} . In addition, a very weak band is observed at 125 cm^{-1} which is assigned to the first member of the $S_4 \nu_5(\tau_{2g})$ progression on the origin, enabled by a very weak Jahn-Teller effect. Just as for the spin forbidden transition, a peak at 38 cm^{-1} lower energy than the origin (in this case, of ${}^7F_6 \Gamma_{1g} \rightarrow {}^7D \Gamma_{4u}$) is observed [dashed line in Fig. 4(a)], for which the intensity increases with temperature, and it is analogously assigned. Another hot origin is observed in 20 K spectrum [dotted line in Fig. 4(a)] and is identified as the absorption from the ${}^7F_6 a \Gamma_{5g}$ level, which is 76 cm^{-1} above the ground state, to the ${}^7D \Gamma_{4u}$ state. On warming from 10 K to 30 K the ZPL show a blueshift of about 12 cm^{-1} [Fig. 4(a)].

Saturation is observed in the 10 K spectrum of $\text{Cs}_2\text{NaTbCl}_6$ [Fig. 4(b)]. A group of well-resolved bands lo-

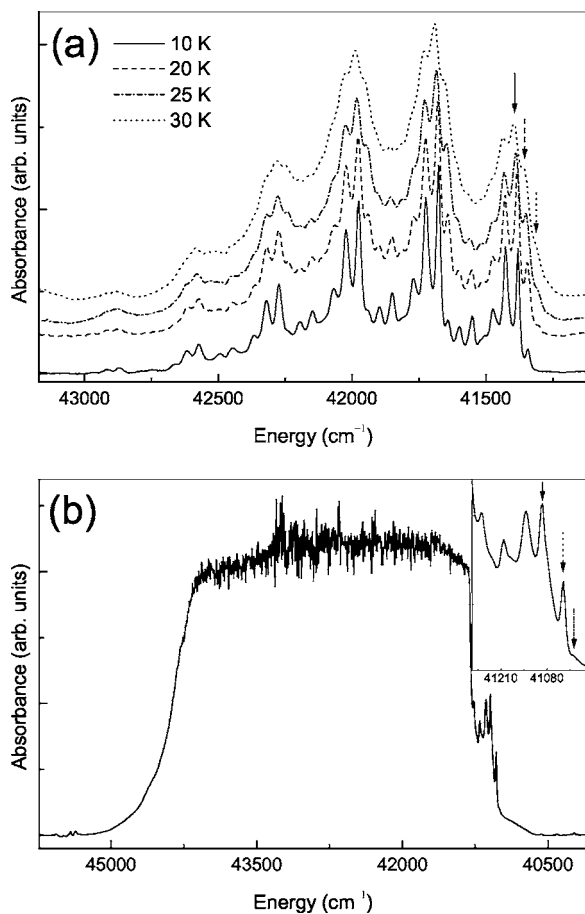


FIG. 4. Absorption spectra of spin-allowed transition in (a) $\text{Cs}_2\text{NaYCl}_6:\text{Tb}^{3+}$ (0.01 mol %) at different temperatures and (b) $\text{Cs}_2\text{NaTbCl}_6$ at 10 K. Refer to the text for bands marked with arrows.

cated around 41 000–41 200 cm^{-1} [shown in the inset of Fig. 4(b)], is assigned to hot transitions. Three origins (marked with arrows) have been identified at 41 004 cm^{-1} (dashed), 41 034 cm^{-1} (dotted), and 41 093 cm^{-1} (solid). The first two origins (41 004 and 41 034 cm^{-1}) are assigned as the ${}^7F_6\Gamma_{3g} \rightarrow {}^7D\Gamma_{4u}$ and ${}^7F_6\Gamma_{5g} \rightarrow {}^7D\Gamma_{4u}$ hot transitions, respectively. The energy differences of these two origins to the ${}^7F_6\Gamma_{1g} \rightarrow {}^7D\Gamma_{4u}$ origin are 376 and 346 cm^{-1} , which are in good agreement with the energies obtained from previous studies.^{13,16} The band at 41 093 cm^{-1} is assigned to ${}^7F_6\Gamma_{1g} + \nu_1 \rightarrow {}^7D\Gamma_{4u}$. The energy of the $S_1(\nu_1)$ vibration obtained from the 20 K Raman spectrum is 290 cm^{-1} . The other (unmarked in the inset) bands at higher energy belong to the progressions upon these mentioned bands. The weak features at both sides of the $4f \rightarrow 5d$ absorption band correspond to the intraconfigurational $f \rightarrow f$ transitions of Tb^{3+} .

C. Vibrational progressions of $4f^8 \rightarrow 4f^75d^1$ transitions

Vibrational progressions have been identified for both spin-forbidden and spin-allowed $4f^8 \rightarrow 4f^75d^1$ transitions of TbCl_6^{3-} . The transformation properties of the major progression modes are restricted to the totally symmetric representations by selection rules at the O_h crystal site of Tb^{3+} . It is

evident however that the progression modes of ~ 48 and $\sim 170 \text{ cm}^{-1}$ are not zone center modes. The energy of the $S_1(\nu_1)$ progression mode is not very different from that in the electronic ground state. The fittings of the intensities of the progressions in both the $S_1(\nu_1)(\text{Tb}-\text{Cl})$ and $\nu(\text{lattice})$ to standard equations¹⁹ gives bond length displacements between the $4f^8$ and $4f^75d^1$ configurations Δr , about $5.5 \pm 0.5 \text{ pm}$ for both spin-allowed and forbidden transitions, which is $< 2\%$ change in Tb-Cl bond distance.

Although this bond length change is small, its sign has received considerable attention from *ab initio* calculations.²⁰ The change in bond distance upon $f-d(t_{2g})$ excitation has been calculated to be contractive, of magnitude about 4 pm for CeCl_6^{3-} . A contractive bond length change would lead to an increase in the bond force constant and thus to an increase in the vibrational energy. It was not feasible to compare the $S_1(\nu_1)$ vibrational frequency in the ground state and in the $d(t_{2g})$ state of CeCl_6^{3-} because neat $\text{Cs}_2\text{NaCeCl}_6$, for which Raman data are available, exhibits total absorption for the $f-d$ transitions so that the diluted system $\text{Cs}_2\text{NaYCl}_6:\text{Ce}^{3+}$ was studied. The comparison between ground state and excited state vibrational frequencies can be clearly made for the spin-forbidden $f-d(t_{2g})$ transition of $\text{Cs}_2\text{NaTbCl}_6$. As mentioned above, the $S_1(\nu_1)$ ground-state frequency at 20 K is 290 cm^{-1} . From the lowest energy and the highest energy bands in Fig. 3(b) the $S_1(\nu_1)$ progression frequency is measured as $298 \pm 2 \text{ cm}^{-1}$, which is an indication of the bond length contraction upon excitation.

IV. CALCULATIONS

A. Simple model analysis of $4f^75d$ energy levels

Not all of the interactions for the $4f^{N-1}5d$ configurations are of the same importance. Generally, the strengths of the Coulomb interaction for the $4f^{N-1}$ core and the crystal-field interaction for the $5d$ electron are much larger than other interactions.²¹ The four experimental Γ_{4u} levels of the $4f^75d$ configuration are expected to arise from the coupling of the $4f^7$ core state 8S with the $5d^1 {}^2t_{2g}$ state. In the following, we use a simple model to analyze the energy levels associated with the $({}^8S, {}^2t_{2g})$ states.

An approximate effective Hamiltonian for the $4f^75d$ states $({}^8S, {}^2t_{2g})$ can be written as

$$H_{\text{eff}}({}^8S, {}^2t_{2g}) = E_{\text{av}} - J_{\text{ex}}\mathbf{S}_f \cdot \mathbf{s}_d + \zeta_d \mathbf{s}_d \cdot \mathbf{l}_d, \quad (2)$$

where E_{av} is the barycenter energy of the $({}^8S, {}^2t_{2g})$ states and does not contribute to the splitting. The second term is the isotropic exchange interaction between $4f^7$ and $5d$, which splits $({}^8S, {}^2t_{2g})$ into a nonet [$({}^8S) {}^9S, t_{2g}$] and a septet [$({}^8S) {}^7S, t_{2g}$]. The third term represents the spin-orbit interaction of the $5d$ electron, which is smaller in magnitude than the second term and responsible for the splitting of the nonet and septet. Since the quantum number for the total orbital angular momentum of the 8S term is equal to zero, the direct Coulomb interaction between $4f^7$ and $5d$, and the spin-orbit and crystal-field interaction of the $4f$ electrons are negligibly small and thus not included in the effective Hamiltonian.

A schematic representation of the above qualitative energy-level analysis is presented in Fig. 2(a). A evaluation of diagonal matrix element of the isotropic exchange interaction between $[(^8S)^9S, t_{2g}]$ and $[(^8S)^7S, t_{2g}]$ states leads to the eigenvalues $E_{av} - (7/4)J_{ex}$ and $E_{av} + (9/4)J_{ex}$, respectively. These two energies were adjusted with respect to the energies of the first (I) and fourth (IV) observed Γ_{4u} levels, giving $J_{ex} = 1762 \text{ cm}^{-1}$. The nonet and septet are further shifted and split by the spin-orbit interaction of the $5d$ electron into two groups of crystal-field levels with a splitting of 1258 cm^{-1} for each group, as indicated by the shaded areas in Fig. 2(a). This splitting value has been estimated from the relative energies of the first (I) and third (III) observed Γ_{4u} levels. As shown in Fig. 2, the irreducible representations for the two groups of crystal-field levels, which can be readily obtained from reduction of the direct product of representations 9S ($\Gamma_{1u} + \Gamma_{3u} + \Gamma_{4u} + \Gamma_{5u}$), 7S ($\Gamma_{2u} + \Gamma_{4u} + \Gamma_{5u}$), and t_{2g} , contain three Γ_{4u} levels for each group, which is consistent with experimental observations and also with the results from the energy level calculations described in the following subsection.

From the above simple analysis, we know that the splitting of the lowest three observed Γ_{4u} levels is caused by the spin-orbit interaction of the $5d$ electron, and the splitting of the fourth observed Γ_{4u} level relative to the lowest three ones is caused by the f - d isotropic exchange interactions.

B. Calculation of $4f^75d$ energy levels

The energy level calculation employed the extended f -shell programs of Reid, in which the electronic energy levels were calculated by simultaneous diagonalization of various parametrized Hamiltonians for the $4f^75d$ configuration. The details for such calculations can be found in Ref. 22. In the calculation, the values of parameters for the $4f$ electrons, including Coulomb interaction between the $4f$ electrons, spin-orbit interaction, other small atomic interactions, and the crystal-field interaction parameters, were taken from those of $4f^8$ configuration,²³ and were multiplied by a small factor 1.06, as done by van Pieterse *et al.*,⁴ to take into account the slightly larger Coulomb interaction for the contracted $4f^7$ core. The crystal-field parameter for the $5d$ electron is from the fitting to Ce^{3+} crystal-field energy levels in the same host.²⁴ The spin-orbit parameter for the $5d$ electron was adjusted until the best agreement with experimental splitting was obtained for the three lowest Γ_{4u} levels. The f - d interaction parameters were estimated from the standard atomic computer programs,²⁵ but were reduced to 43% of the calculated free ion values in order to predict a correct splitting between the high and low spin state, i.e., the splitting between the experimental I and IV Γ_{4u} levels [see Fig. 2(b)]. This reduction is considerably larger than that for Tb^{3+} with F^- ligands,⁴ which may be linked to the fact that Cl^- is more covalent than F^- . In addition to the splitting into many energy levels due to interactions within the $4f^75d$ configuration, the position of the energy levels is determined by the difference between the average energies of $4f^75d$ and $4f^8$ configurations $\Delta_E(fd)$, since the energy levels of $4f^75d$ and $4f^8$ configurations are simultaneously calculated in the pro-

TABLE II. Energy parameters for $4f^75d$ configuration of Tb^{3+} in $\text{Cs}_2\text{NaYCl}_6$. Parameters for the splitting of $4f^7$ core (such as parameters for Coulomb interaction, spin-orbit interaction, and crystal-field splitting) are obtained from literature and multiplied by 1.06. The parameter for the crystal-field splitting of the $5d$ state was taken from Ref. 24. See Ref. 26 for parameter definitions.

Parameters	cm^{-1}
$F^2(ff)$	94 067
$F^4(ff)$	66 697
$F^6(ff)$	45 964
ζ_f	1797
$\alpha(f)$	18.4
$\beta(f)$	-554.4
$\gamma(f)$	2069.1
$M^0(f)^a$	4.6
$P^2(f)^a$	1007.0
$B_0^4(f)^b$	1821.2
$B_0^6(f)^b$	191.0
ζ_d	1185
$B_0^4(d)^b$	38709
$\Delta_E(fd)$	74004
$F^2(fd)$	12960
$F^4(fd)$	6232
$G^1(fd)$	5367
$G^3(fd)$	4556
$G^5(fd)$	3525

^a $M = 0.56M^0$, $M^4 = 0.31M^0$; $P^4 = 0.75P^2$, $P^6 = 0.1P^2$.

^bThe crystal-field Hamiltonians for the $4f$ and $5d$ electrons are defined as $H_{\text{CF}}(f) = B_0^4(f)[C_0^4 + (\sqrt{5}/\sqrt{14})(C_4^4 + C_{-4}^4)] + B_0^6(f)[C_0^6 - (\sqrt{7}/\sqrt{2})(C_4^6 + C_{-4}^6)]$ and $H_{\text{CF}}(d) = B_0^4(d)[C_0^4 + (\sqrt{5}/\sqrt{14})(C_4^4 + C_{-4}^4)]$.

gram. This energy difference comprises several sources, including kinetic energy, Coulomb and (isotropic) crystal field effects. The influence of $\Delta_E(fd)$ is to shift all the $4f^75d$ energy levels by the same amount relative to the $4f^8$ ground state and $\Delta_E(fd)$ is adjusted to obtain the best agreement between experiment and calculations. The energy parameters used in the calculation of the $4f^75d$ energy levels are collected in Table II.

Some of the calculated energy levels for the $4f^75d$ configuration are listed in Table III and good agreement is obtained with the four experimental levels. It is interesting that the energy levels of both the high- and low-spin groups effectively fall into three groups: refer to Fig. 2(c), Table III. At higher energy ($\sim 53\,600 \text{ cm}^{-1}$, not shown) a further eight of the 9D states are calculated to span only $\sim 100 \text{ cm}^{-1}$, whereas another 5 7D states span $\sim 40 \text{ cm}^{-1}$ near $60\,300 \text{ cm}^{-1}$.

C. Calculation of $4f^8 \rightarrow 4f^75d$ absorption strengths

The transitions from $4f^8$ to $4f^75d$ are electric dipole allowed and the electric dipole matrix elements for the transitions can be calculated using the formulae described in Ref. 27. In the calculation, we made the approximation that the

TABLE III. Calculated and experimental electronic energy levels for the $4f^75d$ configuration of Tb^{3+} in Cs_2NaYCl_6 . Only the relative oscillator strengths in the spectral range of 34 000–43 000 cm^{-1} were calculated.

$4f^75d$ level	Energy (cm^{-1})		Calculated relative oscillator strength from initial state ^a				
	E_{calc}	E_{obs}	${}^7F_6\Gamma_{1g}$	${}^7F_6\Gamma_{4g}$		${}^7F_6a\Gamma_{5g}$	
				10 K	20 K	10 K	20 K
${}^9D\Gamma_{5u}$	34 327		0.00	0.01	0.12	0.00	0.02
${}^9D\Gamma_{3u}$	34 328		0.00	0.00	0.09	0.00	0.00
${}^9D\Gamma_{4u}$	34 332	34332	1.00	0.00	0.03	0.00	0.00
${}^9D\Gamma_{5u}$	34 333		0.00	0.00	0.02	0.00	0.00
${}^9D\Gamma_{2u}$	34 960		0.00	0.00	0.00	0.00	0.02
${}^9D\Gamma_{5u}$	34 962		0.00	0.00	0.07	0.00	0.02
${}^9D\Gamma_{3u}$	34 964		0.00	0.09	1.25	0.00	0.05
${}^9D\Gamma_{4u}$	34 969	34982	1.4	0.01	0.13	0.00	0.03
${}^9D\Gamma_{1u}$	35 599		0.00	0.03	0.43	0.00	0.00
${}^9D\Gamma_{4u}$	35 600	35590	58	0.22	3.19	0.00	0.07
${}^9D\Gamma_{5u}$	35 601		0.00	0.63	9.04	0.00	0.37
${}^7D\Gamma_{3u}$	41 383		0.00	61	879	0.14	46
${}^7D\Gamma_{4u}$	41 386	41380	16305	114	1631	0.09	31
${}^7D\Gamma_{1u}$	41 955		0.00	1.3	19.1	0.00	0.00
${}^7D\Gamma_{4u}$	41 980		1390	20	294	0.00	0.08
${}^7D\Gamma_{5u}$	42 000		0.00	21.6	310	0.07	22
${}^7D\Gamma_{2u}$	42 550		0.00	0.00	0.00	0.00	0.10
${}^7D\Gamma_{5u}$	42 566		0.00	1.6	22.9	0.00	1.2
${}^7D\Gamma_{3u}$	42 576		0.00	7.4	107	0.03	9.4
${}^7D\Gamma_{4u}$	42 611		77	0.01	4.3	0.03	11.2

^aThe energies of ${}^7F_6\Gamma_{4g}$ and ${}^7F_6a\Gamma_{5g}$ were taken as 37 and 81 cm^{-1} , respectively.

unpolarized oscillator strengths f_{if} for the zero-phonon lines between the initial $4f^8$ levels $|f^8\Gamma_i\rangle$ and the final $4f^75d$ levels $|f^7d\Gamma_f\rangle$ are proportional to the total electric dipole transition line strength, multiplied by the zero phonon line transition wave number and a thermal population factor for the initial levels, and can be expressed as

$$f_{if} \propto e^{-E_i/kT} \bar{\nu}_{if} \sum_{q,\gamma_i,\gamma_f} |\langle f^8\Gamma_i\gamma_i | D_q^1 | f^7d\Gamma_f\gamma_f \rangle|^2. \quad (3)$$

Here, the summation is over the polarization q ($q=0, \pm 1$) and the components γ of the initial and final levels.

The derived relative oscillator strengths for the zero phonon lines in the spectral range of 34 000–43 000 cm^{-1} are listed in Table III and are in semiquantitative agreement with experiment. The spin-allowed group of bands is calculated to be about 290 times stronger than the spin-forbidden group at 10 K. Furthermore, only one transition is expected to be observed in the spin-allowed group since the other two transitions involving Γ_{4u} terminal states are 11.7 and 212 times weaker. Concerning the spin-forbidden group, the transition to the origin at 35 590 cm^{-1} is expected to dominate the intensity, although the calculation severely overestimates its intensity ratio with the lowest energy origin (calculated 58:1; experiment 2.1:1). Also, the lowest two transitions are calculated to have the intensity ratio 1.4:1, whereas that observed is 0.8:1. Refinement of the parameters would undoubtedly

lead to a better agreement but we have not performed this due to the paucity of experimental data. It is noted, however, in Table III that the additional intensity at 10 K from hot transitions from the first excited state ${}^7F_6\Gamma_{4g}$ is minor. This is in agreement with our spectra. Second, at 20 K, the additional intensity contributions from the first two excited states are again fairly minor, as in Figs. 2 and 3.

V. CONCLUSIONS

Several advantages have been shown to be forthcoming when studying the $f-d$ spectra of lanthanide ions in high symmetry, rather than in low symmetry, environments. Not only is the energy level scheme simpler, due to higher degeneracies, but selection rules limit the number of allowed transitions between the crystal-field levels. It is also pertinent that the f^8 and the f^7d configurations are unmixed for these centrosymmetric systems because of their opposite parity. Thus, the less-cluttered spectra permit the observation of detailed vibrational structure at low temperatures. Most importantly, the simple spectra permit the assignment of symmetry representations to the terminal d -electron levels.

In this study we have reported the high resolution absorption spectra of Tb^{3+} in hexachloroelpasolite lattices in the region between 34 000–43 000 cm^{-1} . Two sets of $4f^8 \rightarrow 4f^75d^1$ transitions were observed, starting at 34 332

and 41 380 cm^{-1} , and assigned to spin-forbidden and spin-allowed transitions, respectively. The calculated energies and intensities are in semi-quantitative agreement with experiment.

Franck-Condon analysis of the absorption bands showed that the displacement of the $4f^75d^1$ potential energy minimum from that of $4f^8$ is small and that the Tb—Cl bond length change is about 5.5 pm. Consideration of the change in totally symmetric stretching mode vibrational energy in

the excited state provides an indication that the bond shortens slightly in the $d(t_{2g})$ state.

ACKNOWLEDGMENTS

P.A.T. thanks the Hong Kong University Grants Commission for financial support of this work under Research Grant No. 102304. We thank Professor M. Reid for his contribution to the early part of this work.

-
- ¹L. van Pieterse, M. F. Reid, and A. Meijerink, *Phys. Rev. Lett.* **88**, 067405 (2002).
 - ²L. van Pieterse, M. F. Reid, R. T. Wegh, and A. Meijerink, *J. Lumin.* **94-95**, 79 (2001).
 - ³L. van Pieterse, R. T. Wegh, A. Meijerink, and M. F. Reid, *J. Chem. Phys.* **115**, 9382 (2001).
 - ⁴L. van Pieterse, M. F. Reid, R. T. Wegh, S. Soverna, and A. Meijerink, *Phys. Rev. B* **65**, 045113 (2002); **65**, 045114 (2002).
 - ⁵V. F. Zolin, *J. Alloys Compd.* **380**, 101 (2004).
 - ⁶T. Hoshina and S. Kuboniwa, *J. Phys. Soc. Jpn.* **31**, 828 (1971).
 - ⁷J. L. Ryan and C. K. Jørgensen, *J. Phys. Chem.* **70**, 2845 (1966).
 - ⁸W. T. Carnall, P. R. Fields, and K. Rajnak, *J. Chem. Phys.* **49**, 4447 (1968).
 - ⁹J. Shi and S. Zhang, *J. Phys.: Condens. Matter* **15**, 4101 (2003).
 - ¹⁰P. A. Tanner, *Top. Curr. Chem.* **241**, 167 (2004).
 - ¹¹R. W. Schwartz, H. G. Brittain, J. P. Riehl, W. Yeakel, and F. S. Richardson, *Mol. Phys.* **34**, 361 (1977).
 - ¹²L. C. Thompson, O. A. Serra, J. P. Riehl, F. S. Richardson, and R. W. Schwartz, *Chem. Phys.* **26**, 393 (1977).
 - ¹³I. D. Morrison, A. J. Berry, and R. G. Denning, *Mol. Phys.* **96**, 43 (1999).
 - ¹⁴M. Bettinelli and C. D. Flint, *J. Phys.: Condens. Matter* **2**, 8417 (1990).
 - ¹⁵D. M. Moran, P. S. May, and F. S. Richardson, *Chem. Phys.* **186**, 77 (1994).
 - ¹⁶P. A. Tanner, Y. L. Liu, M. Chua, and M. F. Reid, *J. Alloys Compd.* **207/208**, 83 (1994).
 - ¹⁷L. R. Morss, M. Siegal, L. Strenger, and N. Edelstein, *Inorg. Chem.* **9**, 1771 (1970).
 - ¹⁸A. Lentz, *J. Phys. Chem. Solids* **35**, 827 (1974).
 - ¹⁹H. Yersin, H. Otto, J. I. Zink, and G. Gliemann, *J. Am. Chem. Soc.* **102**, 951 (1980).
 - ²⁰Z. Barandiarán, N. M. Edelstein, B. Ordejón, F. Ruipérez, and L. Seijo, *J. Solid State Chem.* **178**, 464 (2005).
 - ²¹L. Ning, C. K. Duan, S. Xia, M. F. Reid, and P. A. Tanner, *J. Alloys Compd.* **366**, 34 (2004).
 - ²²M. F. Reid, L. van Pieterse, R. T. Wegh, and A. Meijerink, *Phys. Rev. B* **62**, 14 744 (2000).
 - ²³A. J. Berry, C. S. McCaw, I. D. Morrison, and R. G. Denning, *J. Lumin.* **66&67**, 272 (1996).
 - ²⁴P. A. Tanner, C. S. K. Mak, N. M. Edelstein, G. Liu, J. Huang, L. Seijo, and Z. Barandiarán, *J. Am. Chem. Soc.* **125**, 13225 (2003).
 - ²⁵R. D. Cowan, *The Theory of Atomic Structure and Spectra* (University of California Press, Berkeley, 1981).
 - ²⁶M. F. Reid, L. van Pieterse, R. T. Wegh, and A. Meijerink, *Phys. Rev. B* **62**, 14744 (2000).
 - ²⁷L. Ning, Y. Jiang, S. Xia, and P. A. Tanner, *J. Phys.: Condens. Matter* **15**, 7337 (2003).